Journal of Engineering Science and Technology
Vol. 18, No. 2 (2023) 827 - 843
© School of Engineering, Taylor's University

STUDY AND ANALYSIS OF METAL PARTS FABRICATED THROUGH FUSED DEPOSITION MODELLING, DE-BINDING AND SINTERING PROCESSES

ABBAS RAZA, KHURRAM ALTAF*,
FAIZ AHMAD, CHOWDHURY A. SHAHED, SYED W. AHMED

Mechanical Engineering Department, Universiti Teknologi PETRONAS,
32610 Seri Iskandar, Perak, Malaysia
*Corresponding Author: Khurram.altaf@utp.edu.my

Abstract

Fused Deposition Modeling being additive manufacturing process is used for making metal, plastics, ceramics, and composite parts as this technology is moldless and creates zero waste material. With less capital investment and simplicity in process, Fused Deposition Modelling has gained attention across the globe for fabricating complex and simple geometry metal parts. 3D printer takes filament as input and extrude green parts which need to be de-bound and sintered for transforming them into metal parts. Thermal de-binding of filament Ultrafuse 316L SS green parts is performed. By varying thermal de-binding parameters including heating rate, holding time and temperature, green parts can be debounded thermally without any defects. The sintered Ultrafuse 316L metal part has achieved maximum tensile strength of 560 MPa, hardness 189 HV and density of 7.47 g/cm^3.

Keywords: 316L SS, 3D Printing, Additive manufacturing, FDM.

1. Introduction

In today's age, AM has added positive evolution in the manufacturing landscape by allowing manufacturers to design and fabricate complex shapes and customized individual products with ease [1]. Moreover, the time from the designing of product to the physical conversion of the part has been reduced and any part can be manufactured easily without the need for mold through AM [2]. For the mass production of metal part components, SLM and EBM have been used primarily in many manufacturing industries to produce metallic parts across the globe [3]. In both processes, the melting of powder metal is done, and this melted powder metal is applied layer by layer for building a physical part as per geometry. Not only high source of energy is required to kickstart the process, but also huge capital investment is needed for the machines [4]. Therefore, a big amount of investment for SLM & EBM is a prerequisite for additive manufacturing of parts. The huge capital investment in these machines and the health risks for the employees by using raw material as metal powder discourage their usage as these add more harm than benefit [5].

A new approach for building metal parts is being developed, which is known as FDM, and it has been also known as FFF or FLM [6]. The most widely used additive manufacturing [7] process, FDM [8] works on the principle of melting thermoplastic filament and extruding molten metal composite layer by layer through nozzle on a predefine path. The heated filament in the form of semi-liquid or paste is to be extruded as per CAD file instructions through the nozzle on the printing bed [6]. Filament is a metal polymer composite which has powder particles and polymer. The thermoplastic polymer as a binder exists among powder particles in the filament. Moreover, another binder exists which is also known as backbone or secondary binder, and it is responsible of retaining part geometry throughout the process from filament to the final part [9].

FDM made green parts undergo MIM post processes for transforming a green part into white part which is a pure metal. The polymer matrix in the green part is being debound through thermal, solvent, or catalytic de-binding process [10, 11]. While de-binding the green part, there might be some defects on the part surface. When the de-binding process is too fast, bubbles and cracks appear on the part surface [12]. De-binding process yields brown part in which primary binder has been evaporated. This brown part will be undergoing through sintering process which evaporates remaining backbone binder and rest of part experiences volume shrinkage, and this shrinkage is between 15% and 20% [13]. After sintering process, the pure metal part is known as silver part or white part.

Liu et al. [14] used FDM approach for printing 316L SS material with binders filament. After sintering, FDM made parts have been transformed into silver parts. The FDM and Sintering parts have been compared with AISI 316L type parts. The tensile strength of FDM and Sintering process parts is comparatively low. Gong et al. [15] used SLM and FDM methods for printing BASF 316L SS parts and mechanical properties including tensile strength, hardness and microstructure were compared. In this study, it was found that FDM made parts have low mechanical properties. Caminero et al. [16] used BASF Ultafuse 316L SS for printing using FFF approach. In this study, Caminero used different build orientations including on-edge, flatwise and upright and found that flatwise and on-edge build orientations have exhibited high mechanical strength.

Tosto et al. [17] took Ultrafuse 316L by BASF & 17-4PH by Markforged filament materials for investigating the characteristics of green and sintered parts using FFF. Flatwise part shows shrinkage of 20% in XY plane, while 25.20% shrinkage in Z direction. The printed parts in upright orientation showed higher anisotropic behavior. Cost Analysis was performed between FFF and SLM for Ultrafuse 316L SS. The cost for part using FFF is significantly low than part fabricated through SLM. Carminati et al. [18] made 316L SS filament green samples using Ultimaker 5S 3D Printer and de-bound the green samples using catalytic de-binding process and sintered under argon atmosphere. The tensile strength of sintered parts in the range of 405 to 450 MPa.

In the past, expensive technologies like EBM and SLM have been adopted for fabricating metal parts and manufactured parts having good mechanical properties. The overall manufacturing cost of fabricating metal parts using above-mentioned technologies is high because of the required high energy source [19]. Hybrid metal/polymer composite filaments have become subject of interest due to the increasing trend of 3D printing technology in these days [20]. A cost-effective [21, 22] and waste free [23] process for fabricating pure metal parts is FDM and its subsequent processes. The green part, which is formed by FDM based process, is gone through subsequent MIM de-binding and sintering processes for removing binder from the part and densifying the silver part [24].

As per BASF, catalytic de-binding is the best suited process for de-binding of Ultrafuse 316L SS green parts. Since capital investment is huge in making a setup of catalytic de-binding and high risk [25] is associated in handling this catalytic de-binding process. In past literature [5, 16, 17, 26, 27], catalytic de-binding of Ultrafuse 316L SS green parts is performed by outsourcing BASF recommended de-binding and sintering service providers. In this study, an attempt has been made for removing binder from the green part by only thermal de-binding process. Moreover, a meticulous research work has been performed by varying de-binding and sintering parameters for optimizing the mechanical strength of sintered metal part.

2. Methods

The commercially available metal polymer composite filament Ultrafuse 316L SS having 2.85 mm diameter of BASF company is selected for this research study. The filament has approximately 90% of stainless-steel powder by weight and remaining 10% consists of primary binder and backbone binder [28]. The density of metal polymer composite filament is 4.86 g/cm^3.

The filament Ultrafuse 316L SS is fed in Ultimaker S5 3D metal printer. With 3D printer, the green part in dog-bone shape is made according to BASF recommended printing parameters [29]. The input instructions are given through a CAD file. The Ultimaker 3D printer is FDM based, and printing is done as per parameters given Table 1.

The green part contains powder metallic particles and binders. The green parts have been made using FDM technology. In FDM, the CAD file of desired part to be taken as an input of instructions and filament which consists of metallic particles and binder is to be fed through filament driver and then nozzle extrudes the heated filament as per CAD file instructions over the printing bed can be seen in Figs. 1(a) and (b). This is how 3D objects have been formed using FDM technology.

Table 1. Printing parameters.

Parameter	Value
Build Orientation	Flatwise
Infill pattern	Hatch $+45^0$
Infill density (%)	100
Bed temperature (°C)	100
Nozzle temperature (°C)	230
Layer thickness (mm)	0.2

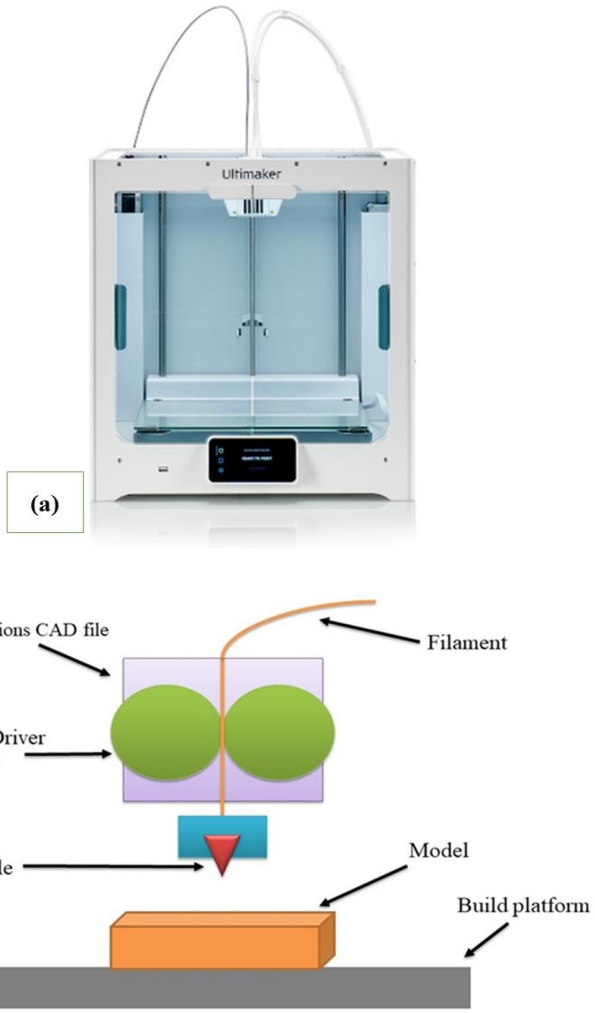

Fig. 1. (a) Ultimaker 5S 3D printer [30], (b) Working principle of FDM.

Once the green parts have been made using FDM technology. The green parts have loosely bound stainless steel powder particles and binder which hold together powder particles. The green parts have been printed as per dimensions in mm mentioned in Fig. 2(a) and isometric CAD model is in Fig. 2(b).

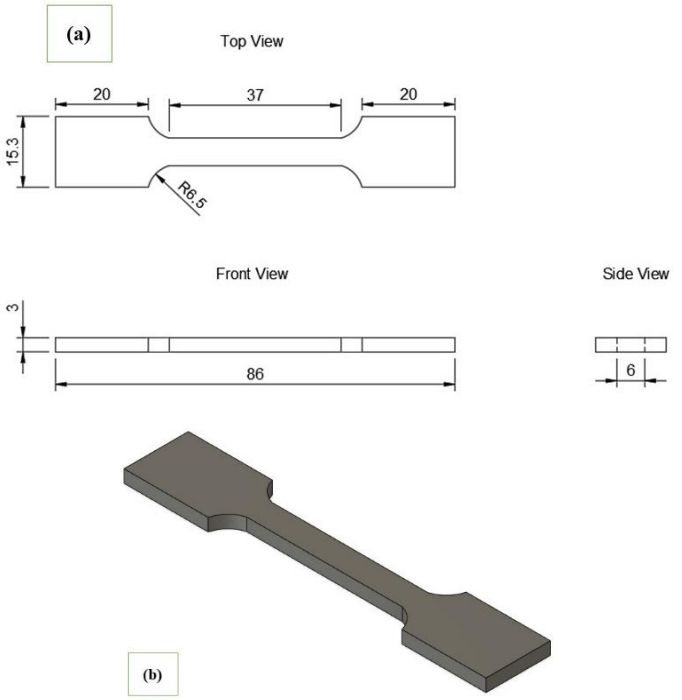

Fig. 2. (a) Geometry of green part, (b) Isometric CAD model

For removing the binder from the green parts, these parts underwent de-binding process. The de-binding process includes thermal de-binding, solvent de-binding, and catalytic de-binding [31] as shown in Fig. 3.

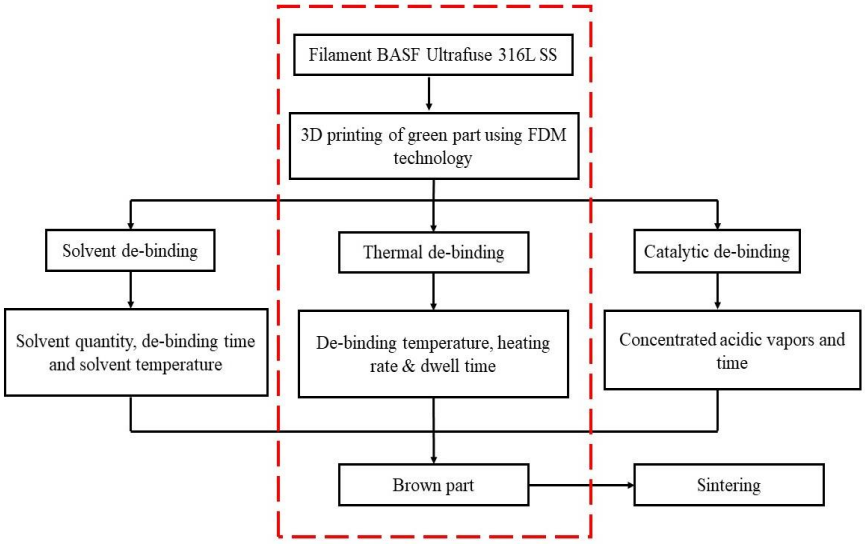

Fig. 3. Techniques for extracting binder from green parts [5].

Out of 3 de-binding techniques, thermal de-binding is adopted for extracting the binder content from the green part. Once the defect free brown parts have been made through thermal de-binding process, the brown parts which consist of loosely metallic particles along with backbone binder is set for sintering. The thermal de-binding parameters are de-binding temperature, heating rate and holding time. The thermal de-binding and sintering of green and brown parts have been performed in tube furnace GSL 1700X by MTI corporation as shown in Fig. 4.

Fig. 4. Tube furnace.

After the sintering process, the stainless-steel powder particles have been fused together and formed a solidified and densified silver part.

Thermal de-binding cycle

The thermal de-binding temperature, heating rate and dwell time can be determined using TGA. With TGA curve in Fig. 5, the critical temperature ranges at which binder starts decomposing and complete decomposition temperature of binder determined. The heating rate should be slow than this critical temperature range and having high holding time could avoid any burn off binder [15]. Therefore, it is suggested that the heating rate should be slow and high critical temperature range what determined during TGA for preventing defects in the part.

From Fig. 5, it is evident that binder melting temperature is starting at around 220 ˚C and decomposition temperature is around 315 ˚C. The binder in the green part will be removed in this given temperature range. Within this temperature range, the heating rate should be kept as low as possible and dwell time should be kept high for the maximum removal of binder from the green part. Using this TGA report of green part, the thermal de-binding parameters have been formulated accordingly.

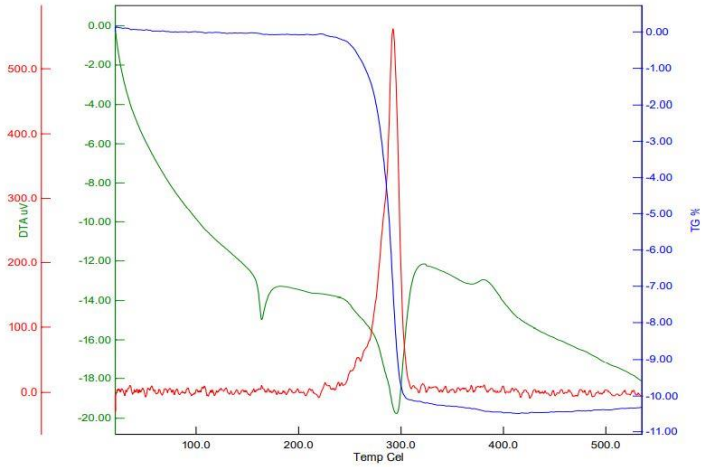

Fig. 5. TGA-DTA-DTG curves of a green part.

3. Results and Discussions

While doing thermal de-binding of green parts, some experiments have been performed for finding the parameters (de-binding temperature, heating rate and holding time) on which defect free brown parts have been made. Moreover, the de-binding temperature, heating rate and holding time have been found as mentioned in Table 2, on which maximum interconnected porosity (removal of primary binder) is created inside the brown part. This brown part has enough strength that it cannot be fractured while handling the fragile part for the sintering process.

In this study, the mass of green and brown parts measured using Brifit digital mini scale as it can be seen in Figs. 6(a) and (b). In doing so, i found that when the mass loss is above 10.5%, the brown part is too fragile that it could not be able to retain it structure and shape. The % mass loss does not impact over shrinkage of final part. When the mass loss is above 10%, either brown part is damaged while handling for sintering or brown part structure is being damaged while taking out from furnace shown in Figs. 7(a) and (b). The optimized parameters are de-binding temperature 310 ˚C, heating rate 1 ˚C /min and holding time 15 minutes for making a defect free brown part as mentioned in Table 2.

$$\% \text{ Mass loss} = \frac{Mg - Mb}{Mg} \times 100 \quad (1)$$

Table 2. Mass loss of green parts.

Sample #	De-binding Temperature (˚C)	Heating Rate (˚C/min)	Holding time (min)	Mass Green Part (g)	Mass brown part (g)	%Mass loss
1	330	2	60	13.80	11.98	13.28
2	330	1	60	13.2	11.72	11.21
3	320	1	60	13.6	11.88	11.07
4	320	1	30	13.3	11.94	10.22
5	315	1	30	13.36	12.05	9.8
6	315	1	15	12.57	11.39	9.37
7	315	1	15	12.90	11.68	9.42
8	310	1	15	12.83	11.64	9.27
9	310	1	10	12.74	11.59	8.98
10	305	1	15	13.6	12.66	7.64

Fig. 6. Mass measurement of (a) green, (b) brown part.

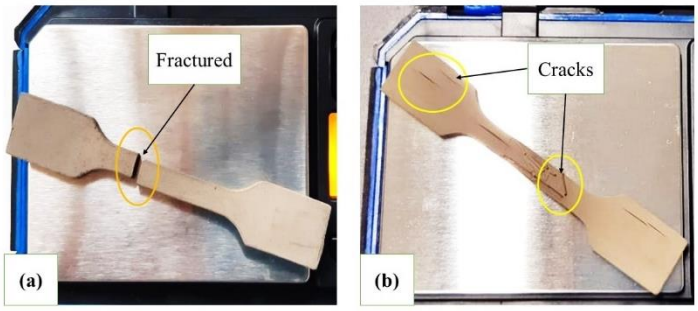

Fig. 7. (a) Fractured, (b) Cracked brown parts.

Furthermore, SEM is performed for observing the internal elements of filament and brown part sample. SEM of filament depicts that SS powder particles are bounded together with binder and binder is removed among the metal particles in SEM of brown part as shown in Figs.8 (a) and (b).

After the de-binding process, the brown part is set to sinter for converting into fully metallic dense part. In this study, Sample 1 is gone through sintering cycle as mentioned in Fig. 9(a), while 3 samples have gone through sintering cycle which is shown in Fig. 9(b).

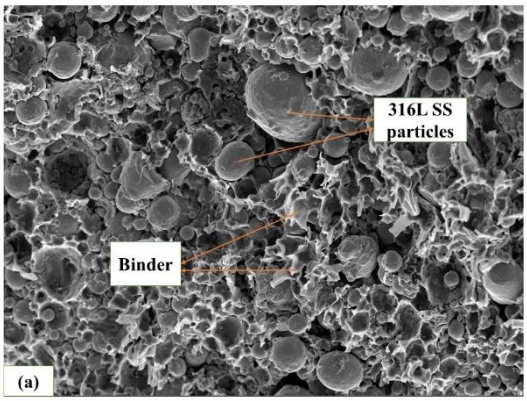

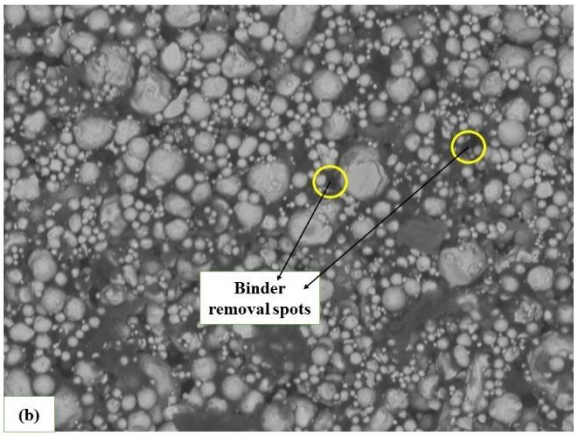

Fig. 8. (a) SEM of (a) filament, (b) brown part.

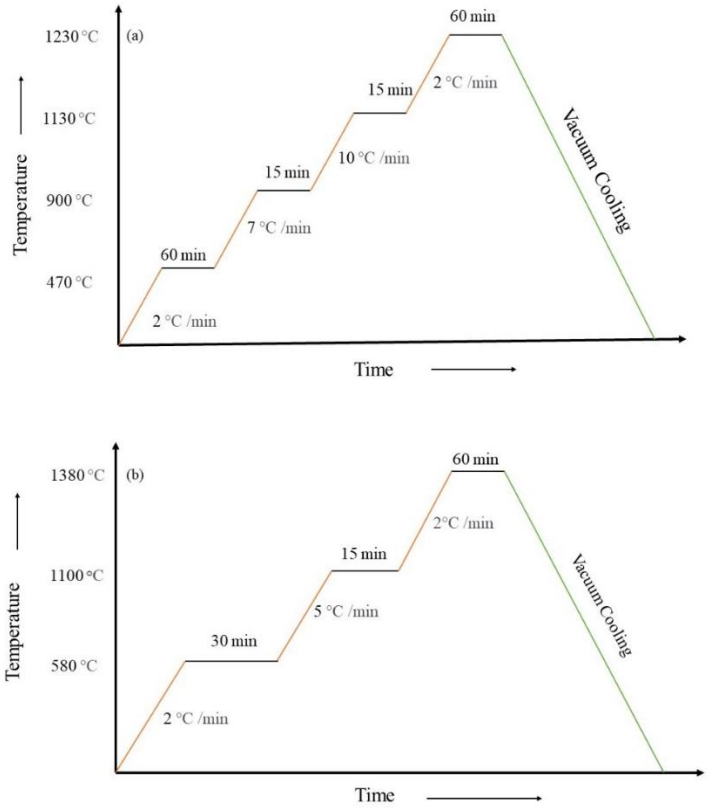

Fig. 9. Sintering cycle of (a) S1[29], and (b) S2, S3, and S4.

All samples have been sintered in furnace GSL 1700X under vacuum from -0.05 MPa to -0.1 MPa. The density, hardness and shrinkage of sintered samples have been measured for observing the impact of sintering parameters.

3.1. Density measurement of sintered parts

The density of sintered metallic part is measured on AX205 balance by METTLER TOLEDO according to ASTM B962-17 [32] is based on Archimedes' principle. Firstly, the dry weight of samples is recorded while sample immersed in fluid and their weight is recorded. The density is calculated using the relation given below [33] as in Eq. (2):

$$\rho = \frac{A}{A-B}(\rho_o - \rho L) + \rho L \quad (2)$$

3.2. Hardness of sintered parts

The hardness of a sintered part is measured according to ASTM E140-02 and equipment leco LM 247AT Vicker hardness tester. The indenter in this equipment formed a diamond pyramid shape indent on the surface of sintered sample parts. The Vicker hardness test is performed with a test load of 100N, and dwell time was used for 10 seconds. The hardness of sintered samples is calculated through formula [34] given in Eq. (3) and mentioned in Table 3:

$$HV = \frac{1.854P}{d^2} \quad (3)$$

3.3. Shrinkage analysis of sintered parts

The shrinkage percentage can be done on length, width, and thickness. The dimensions of the green part have been taken as reference for determining the shrinkage effect on the sintered metallic part. The shrinkage [35] percentage Eq. (4) is:

$$\% \text{ Shrinkage} = \big((Lg - Ls)/Lg\big) \times 100 \quad (4)$$

Table 3. Hardness, density and shrinkage of sintered parts.

Sample #	Hardness (HV)	Density (kg/m^3)	Shrinkage %
1	245	7120	12
2	197	7380	17.1
3	192	7470	17.7
4	189	7410	16.8

3.4. Tensile strength of sintered parts

Tensile test was performed on sintered metallic 316L SS parts on UTM Amsler Zwick 100 kN according to ASTM E8M [32] with strain rate 1mm/min. All tests were performed at room temperature and 50% humidity level. This testing machine has load cells and extensometer for gauging extension. The Tensile strength and Elongation at break of sintered samples are mentioned in Figs. 10(a) and 10(b).

3.5. Grain structure of sintered parts

To observe the grain structure of sintered samples, the samples have been grinded through sandpaper of 60 grit to 4000 grit. The grinded samples have been polished with polycrystalline polish of 6µm, 3µm and 1µm. After polishing, the sintered samples have gone through electrolytic etching. The etchant is oxalic acid 10% by volume, electric voltage was 2 V-5 V and performed for 15 to 30 seconds on the surface to be investigated. As etching is performed, the grain structure is seen

thorough optical microscope Leica with 200 µm resolution as in Figs. 11(a) and (b). Since samples 2, 3, and 4 have undergone same sintering cycle, only grain structure of sample 2 is presented here:

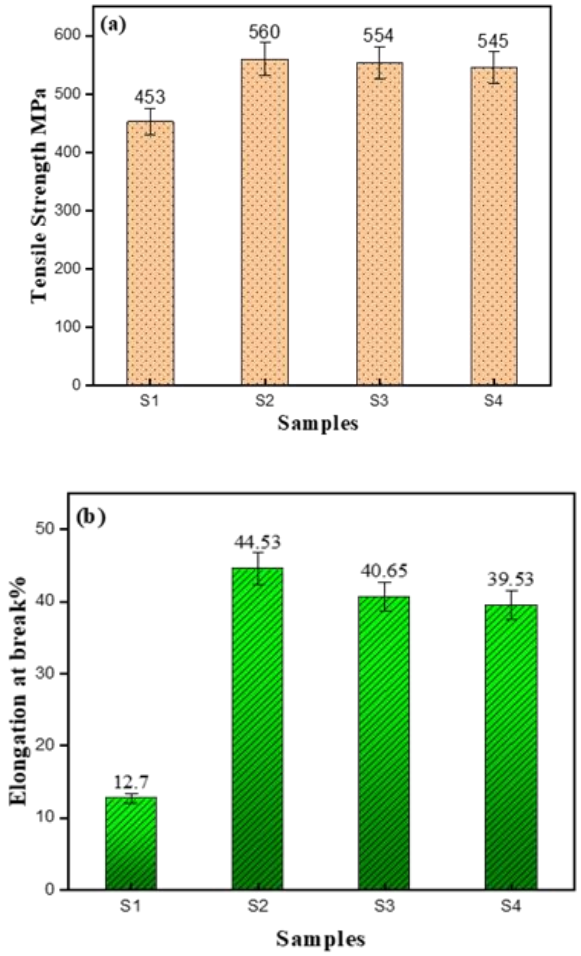

Fig. 10. (a) Tensile strength, (b) Elongation at break of sintered parts.

3.6. Grain structure of sintered parts

From Fig. 12(a), it is evident that this sample underwent brittle fracture. This type of fracture occurs suddenly in the material without exhibiting any major structural deformation and warning. Furthermore, from the grain structure of sample 1, it appears that grain size is smaller than the grain size of samples 2, 3, and 4. The lesser grain boundaries in the grain structure have reduced the mechanical strength of sample 1 as it can be seen in Fig. 11(a). The lack of visible grain boundaries depicts those grains could not withstand high stress. Moreover, pores are more in sample 1 and density is less of this sample in comparison to other samples. The lack of grain boundaries along with high porosity in sample 1 are responsible for brittle fracture.

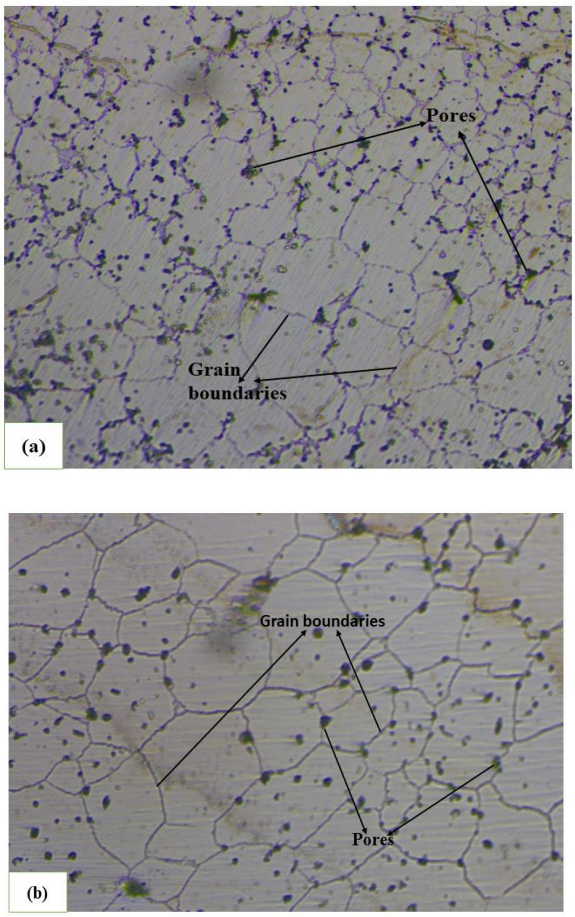

Fig. 11. Grain structure of (a) Sample 1, (b) Sample 2.

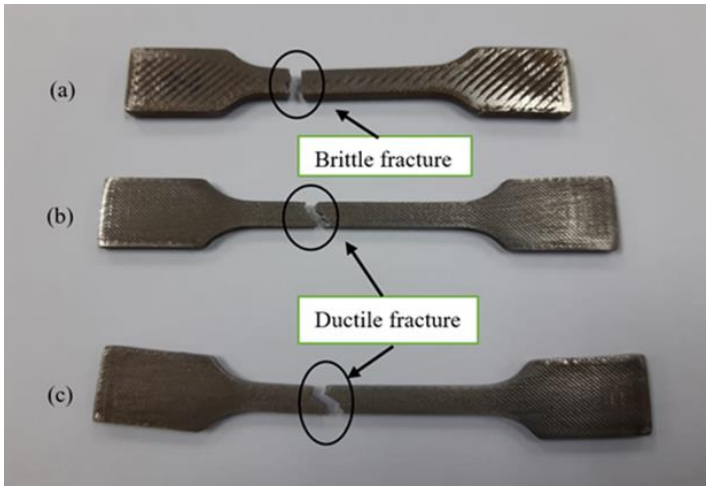

Fig. 12. (a) Sample 1 (b) Sample 2, and (c) Sample 3.

The fracture in samples 2, 3, and 4 is ductile as this can been seen in Rocha-Rangel work [36]. In this type of fracture, plastic deformation phase sounds the alarm that failure in the material is to be occurred soon [37]. In this sample, the porosity is relatively low in comparison to sample 1.

The less porosity makes the sample denser. Moreover, the grain boundaries are clearer as shown in Fig. 11(b). The clear and large number of grain boundaries indicate that grains have more strength and could bear high stress load. The less porosity, more grain boundaries and elevated sintering temperature have increased ductility in these sample in comparison to sample 1. Not only ductility but also mechanical strength of samples has been enhanced.

With these de-binding and sintering parameters, the brown part being sintered and yielded SS dog-bone sample which will show extensive plastic deformation behavior before going to be fractured. The samples 2, 3, and 4 have been sintered with high sintering temperature which is 1360 ˚C, while sample1 has sintering temperature 1230 ˚C. Samples 2, 3, and 4 have more time for the diffusion of metal particles under elevated temperature in comparison to sample 1. The high diffusion time among the metal particles yields high mechanical strength. Sample 1 has shown less shrinkage and has low density while samples 2, 3, and 4 have exhibited above 17% shrinkage and have high density. At elevated sintering temperature and high diffusion time among the metal particles, samples 2, 3, and 4 have been sintered with high density. While sample 1 has low sintering temperature and less diffusion time for metal particles. Therefore, sample 1 has low density in comparison to samples 2, 3, and 4.

4. Conclusions

The appropriate thermal de-binding cycle and sintering cycle have been found in this study for BASF Ultrafuse 316L SS green parts made using FDM process. The appropriate mass loss in de-bound part through thermal de-binding process is around 9 to 10%. The densified stainless-steel part 7470 kg/m^3 having good shrinkage approximately 17% along the thickness, with hardness of 189 HV having tensile strength of 560 MPa is achieved using the optimized sintering cycle. The maximum achieved elongation at break was 44.53% in this study. This factor can be enhanced by further varying the sintering parameters. In the given scenario, the maximum tensile strength of 560 MPa is achievable. Using FDM as an economical approach, SS parts can be printed, and subsequent processes can be applied using optimized parameters. Therefore, this process can enhance the mechanical strength of silver parts.

5. Future Recommendations

In the wake of silver parts made through FDM and subsequent processes, it is pertinent to mention that ductility and elongation at break of silver parts need to be enhanced. Sintering parameters under Hydrogen and Argon gas atmosphere need to be varied for investigating the influence over mechanical strength, ductility, and other characteristic of silver parts. The fracture analysis of metal parts made through FDM, and subsequent processes needs to be investigated comprehensively. A practical metal application like metal nut and bolt or fins, made through FDM and subsequent processes to be gauged and compared with conventional manufacturing process made metal application.

Acknowledgement

We are extremely thankful for the Collaborative Research Fund (015MDO-061) and UTP for providing a conducive atmosphere for carrying out this research study.

Nomenclatures

A	Weight of test specimen in air
B	Weight of test specimen in auxiliary liquid
d	Pyramid's diagonal value
HV	Vickers number
Lg	Length of green part
Ls	Length of sintered part
Mg	Mass of green part
Ms	Mass of sintered part
P	Applied Force

Greek Symbols

ρ	Density of specimen
ρ_L	Density of air
ρ_o	Density of auxiliary liquid

Abbreviations

AM	Additive Manufacturing
ASTM	American Society for Testing and Materials
BASF	Badische Anilin- und SodaFabrik
CAD	Computer Aided Design
DTA	Differential Thermal Analysis
DTG	Derivative Thermogravimetry
EBM	Electron Beam Melting
FDM	Fused Deposition Modelling
FFF	Fused Filament Fabrication
FLM	Fused Layer Modelling
MIM	Metal Injection Moulding
PM	Powder Metallurgy
PIM	Powder Injection Moulding
SLM	Selective Laser Melting
SEM	Scanning Electron Microscopy
TGA	Thermogravimetric Analysis

References

1. Tuncer, N.; and Bose, A. (2020). Solid-state metal additive manufacturing: A review. *JOM*, 72(9), 3090-3111.
2. Schiltz, J; Render, T; Gatrell, B.A.; Qu, H.; Steiner, C.; McGinn, P.; Schmid, S. (2020). Wear behavior of additive manufactured zirconia. *Procedia Manufacturing*, 48, 821-827.

3. Seifi, M.; Salem, A.; Beuth, J.; Harrysson, O.; and Lewandowski, J.J. (2016). Overview of materials qualification needs for metal additive manufacturing. *JOM*, 68(3),747-764.
4. Wischeropp, T.M.; Tarhini, H.; and Emmelmann, C. (2020). Influence of laser beam profile on the selective laser melting process of AlSi10Mg. *Journal of Laser Applications*, 32(2), 022059.
5. Moritzer, E.; Elsner, C.L.; and Schumacher, C. (2021). Investigation of metal-polymer composites manufactured by fused deposition modeling with regard to process parameters. *Polymer Composites*, 42(11), 6065-6079.
6. Rafiee, M.; Farahani, R. D.; and Therriault, D. (2020). Multi-material 3D and 4D printing: A survey. *Advanced Science*,7(12), 1-26.
7. Sadaf, M.; Bragaglia ,M.; and Nanni, F. (2021). A simple route for additive manufacturing of 316L stainless steel via fused filament fabrication. *Journal of Manufacturing Processes*, 67, 141-150.
8. Ngo, T.D.; Kashani, A.; Imbalzano, G.; Nguyen, K.T.Q.; and Hui, D. (2018). Additive manufacturing (3D printing): A review of materials, methods, applications and challenges. *Composites Part B*, 143, 172-196.
9. Miranda, R. (2013). *Handbook of metal injection molding*. Routledge.
10. Hamidi, M.F.F.A.; Harun, W.S.W.; Khalil, N.Z. ; Ghani, S.AC. ; and Azir, M.Z. (2017). Study of solvent debinding parameters for metal injection moulded 316L stainless steel. *IOP Conference Series: Materials Science and Engineering*, 257, 012035.
11. Krueger, D.C. (1995). Process for improving the debinding rate of ceramic and metal injection molded products. United States Patent US5531958A
12. .Supriadi, S.; Suharno, B.; Hidayatullah, R. ; Maulana, G. ; and Baek, E.R. (2017). Thermal debinding process of SS 17-4 PH in metal injection molding process with variation of heating rates, temperatures, and holding times. *Solid State Phenomena*, 266, 238-244.
13. Charlon, S.; Le Boterff, J.; and Soulestin, J. (2021). Fused filament fabrication of polypropylene: Influence of the bead temperature on adhesion and porosity. *Additive Manufacturing*, 38, 101838.
14. Liu, B.; Wang, Y.; Lin, Z.; and Zhang, T. (2020). Creating metal parts by fused deposition modeling and sintering. *Material Letters*, 263, 127252.
15. Gong, H.; Snelling, D.; Kardel, K.; and Carrano, A. (2019). Comparison of stainless steel 316L parts made by FDM - and SLM-Based additive manufacturing processes. *JOM*, 71(3), 880-885.
16. Caminero, M.A.; Romero, A.; Chacón, J.M.; Núñez, P.J.; García-Plaza, E.; and Rodríguez, G.P. (2021). Additive manufacturing of 316L stainless-steel structures using fused filament fabrication technology: mechanical and geometric properties. *Rapid Prototype Journal*, 27(3), 583-591.
17. Tosto, C.; Tirillo, J.; Sarasini, F.; and Cicala, G. (2021). Hybrid metal/polymer filaments for fused filament fabrication (FFF) to print metal parts. *Applied Sciences*,11(4), 1444.
18. Carminati, M.; Quarto, M.; D'Urso, G.; Giardini, C.; and Maccarini, G. (2022). Mechanical characterization of AISI 316L samples printed using material extrusion. *Applied Sciences*, 12(3), 1433.

19. Gonzalez-Gutierrez, J.; Cano, S.; Schuschnigg, S.; Kukla, C; Sapkota, J.; and Holzer, C. (2018). Additive manufacturing of metallic and ceramic components by the material extrusion of highly filled polymers: a review and future perspectives. *Materials*, 11(5), 840.
20. Arumugam, G.; Lavanya Priya K.P.; Kusomo, C.M.L.; and Mari, T. (2021). A systemeatic review and analysis of 3D Printed buidling envelopes inspired by nature. *Journal of Engineering Science and Technology* (*JESTEC*), Special issue, 58-73.
21. Saringi, M.I.M.; Masood, S.H.; Palanismay, S.; Jayamani, E.; and Kapoor, A. (2021). Additive Manufacturing of an automobile brake pedal by metal fused deposition modelling. *Materials Today: Proceedings*, 45 (Part 6), 4601-4605.
22. Thompson, Y.; Gonzalez-Gutierrez, J.; Kukla, C.; and Felfer, P. (2019). Fused filament fabrication, debinding and sintering as a low-cost additive manufacturing method of 316L stainless steel. *Additive Manufacturing*, 30, 10086.
23. Kotlinski, J. (2014). Mechanical properties of commercial rapid prototyping materials. *Rapid Prototyping Journal*, 20(6), 499-510.
24. Suwanpreecha, C.; and Manonukul, A. (2022). A Review on material extrusion additive manufacturing of metal and how it compares with metal injection moulding. *Metals*, 12(3), 429.
25. BASF (2022). Retrieved October 12, 2022. from https://forward-am.com/material-portfolio/ultrafuse-filaments-for-fused-fialments-fabrication-fff/metal-fialments/ultrafuse-316l/
26. Jiang, D.; and Ning, F. (2022). Anisotropic deformation of 316L stainless steel overhang structures built by material extrusion based additive manufacturing. *Additive Manufacturing*, 50, 102545
27. Quarto, M.; Carminati, M.; and D'Urso, G. (2021). Density and shrinkage evaluation of AISI 316L parts printed via FDM process. *Materials and Manufacturing Processes*, 36(13), 1535-1543.
28. BASF Ultrafuse 316L Filaments (2022), Retrieved August 06, 2022. from https://shop3duniverse.com/collections/basf-ultrafuse-316l
29. BASF (2019). Retrieved August 06, 2022. from https://www.basf.com/global/en/who-we-are/organization/locations/europe/german-companies/basf-3d-printing-solutions-gmbh/metal-solutions/Ultra fuse_316L.html.
30. Matterhackers (2022). Retrieved October 12, 2022. from http://www.matterhackers.com.
31. Damon, J.; Dietrich, S.; Gorantla, S.; Popp, W.; Okolo, B.; and Schulze, V. (2019). Process porosity and mechanical performance of fused filament fabricated 316L stainless steel. *Rapid Prototyping Journal*, 25(7), 1319-1327.
32. Altaf, K.; Qayyum, J.; Rani, A.M.; Ahmad, F.; Megat-Yusoff, P.S.M.; Baharom, M.; Aziz, A.R.; Jahanzaib, M.; and German, R. (2018). Performance analysis of enhanced 3D printed polymer molds for metal injection molding process.*Metals*,8(6), 433.
33. Aslam, M. (2016). *Powder injection molding of modified* 316*l stainless steel for dental implant application*. Ph.D. Thesis. Universiti Teknologi PETRONAS, Malaysia.

34. Ye, H.; Liu, X.Y.; and Hong, H. (2008). Sintering of 17-4PH stainless steel feedstock for metal injection molding. *Material Letters*, 62(19), 3334-3336.
35. BASF (2021). Retrieved August, 06, 2022, from https://forward-am.com/wp-content/uploads/2021/04/UserGuidelines_2021_03_29.pdf.
36. Rocha-Rangel, E. (2011). *Fracture toughness determinations by means of indentation fracture*. IntechOpen.
37. Callister, W.D.; and Rethwisch, D.G. (2018). *Materials Science and Engineering - An Introduction*. (10^{th} ed.). Wiley.